Earthquakes and Structures, Vol. 3, No. 5 (2012) 675-694
DOI: http://dx.doi.org/10.12989/eas.2012.3.5.675

Origin of the anomalously large upward acceleration associated with the 2008 Iwate-Miyagi Nairiku earthquake

Hideo Takabatake* and Motohiro Matsuoka

Department of Architecture, Kanazawa Institute of Technology, Institute of Disaster and Environmental Science 3-1, Yatsukaho, Hakusan City, Ishikawa 924-0838, Japan

(Received April 9, 2011, Revised January 2, 2012, Accepted January 17, 2012)

Abstract. The 2008 Iwate-Miyagi Nairiku earthquake (M_w 6.9, M_{jma} 7.2) occurred on 14 June 2008 in Japan. The amplification and asymmetric waveform of the vertical acceleration at the ground surface recorded by accelerometers at station IWTH25, situated 3 km from the source, were remarkable in two ways. First, the vertical acceleration was extremely large (PGA = 38.66 m/s^2 for the vertical component, PGA = 42.78 m/s^2 for the sum of the three components). Second, an unusual asymmetric waveform, which is too far above the zero acceleration axis, as well as large upward spikes were observed. Using a multi-degree-of-freedom (MDF) system consisting of a one-dimensional continuum subjected to vertical acceleration recorded at a depth of 260 m below ground level, the present paper clarifies numerically that these singular phenomena in the surface vertical acceleration records occurred as a result of the jumping and collision of a layer in vertical motion. We herein propose a new mechanism for such jumping and collision of ground layers. The unexpected extensive landslides that occurred in the area around the epicenter are believed to have been produced by such jumping under the influence of vertical acceleration.

Keywords: vertical motion; 2008 Iwate-Miyagi Nairiku earthquake; unprecedented vertical acceleration; jumping; collision; push up; earthquake resistance

1. Introduction

An extremely singular surface vertical acceleration waveform, which is fundamentally different from those found in previous studies of near-fault ground motions (Tothong and Cornell 2008, Yang *et al*. 2009, Tahghighi 2011), was recorded near the source during the 2008 Iwate-Miyagi Nairiku earthquake (M_w 6.9, M_{jma} 7.2), which occurred on 14 June 2008 in Japan. The source of this earthquake was located at a depth of 8 km in the southern part of Iwate prefecture. Due to this earthquake, numerous mountains near the source experienced extensive landslides at several locations and a large road bridge collapsed vertically, as shown in Figs. 1(a) and 1(b), respectively. Seismic waves associated with this earthquake were recorded by the Kiban-Kyoshin Network (KiK-net), which is operated by the National Research Institute for Earth Science and Disaster Prevention. Among the seismographs in the KiK-net system, two important anomalies with respect to vertical ground surface acceleration were recorded by accelerometers at station IWTH25, which is located

*Corresponding author, Professor, E-mail: hideo@neptune.kanazawa-it.ac.jp

(a) (b)

Fig. 1 Earthquake damage: (a) landslide and (b) collapsed bridge

on a fault at West Ichinoseki station, and is situated 3 km from the source. The ground surface accelerometer of station IWTH25 recorded one of the largest peak ground acceleration (PGA) (42.78 m/s^2 for the vector sum of the three components) ever observed. The first anomaly is that the peak surface vertical acceleration is 38.66 m/s^2, which is nearly 4 G, as shown in Fig. 2(a) and listed in Table 1. On the other hand, the surface horizontal accelerations recorded simultaneously with this vertical acceleration are 11.43 m/s^2 for the NS component and 14.33 m/s^2 for the EW component. Thus, the vertical PGA is extremely large. The second anomaly is an asymmetric waveform with large upward spikes observed in the vertical acceleration record. The upward vertical acceleration is much larger than that in the downward direction.

Station IWTH25 has two accelerometers at the same site. One is in a borehole at a depth of 260 m below ground level (GL-260 m), and the other is on the ground surface. The peak accelerations recorded by the accelerometer set at GL-260 m are 6.81 m/s^2 for the UD component, 10.36 m/s^2 for the NS component, and 7.48 m/s^2 for the EW component, as listed in Table 1. The time histories of these acceleration waves are well-known waveforms, as shown in Figs. 2(d), 2(e) and 2(f), and are symmetric with peak values that are not very large. Table 1 shows the peak acceleration records at both GL-260 m and the ground surface. The amplifications of these accelerations are 5.7, 1.1 and 1.9 times for the UD, NS and EW components, respectively. In addition, the wave propagation velocities from the ground surface to GL-260 m, as revealed by the KiK-net records, are shown in Fig. 3 and listed in Table 2.

It has been reported for previous earthquakes that peak vertical accelerations of greater than 1 G are possible. In this case, when the ground is in an upward movement phase, the effect of gravity is cancelled and the material jumps up when the wave velocity is simultaneously upward. Takabatake *et al*. (2008) showed that the phenomenon of upthrown boulders occurred in the source area for certain large shallow earthquakes because of the pulse-like action of ground shaking; the effect was stronger for vertical than for horizontal oscillations. The likelihood of this phenomenon occurring is greatest when the characteristic period of the earthquake wave matches the vibration period of the ground. Therefore, this phenomenon is attributed to resonance in the dynamic response of the ground to earthquake excitation.

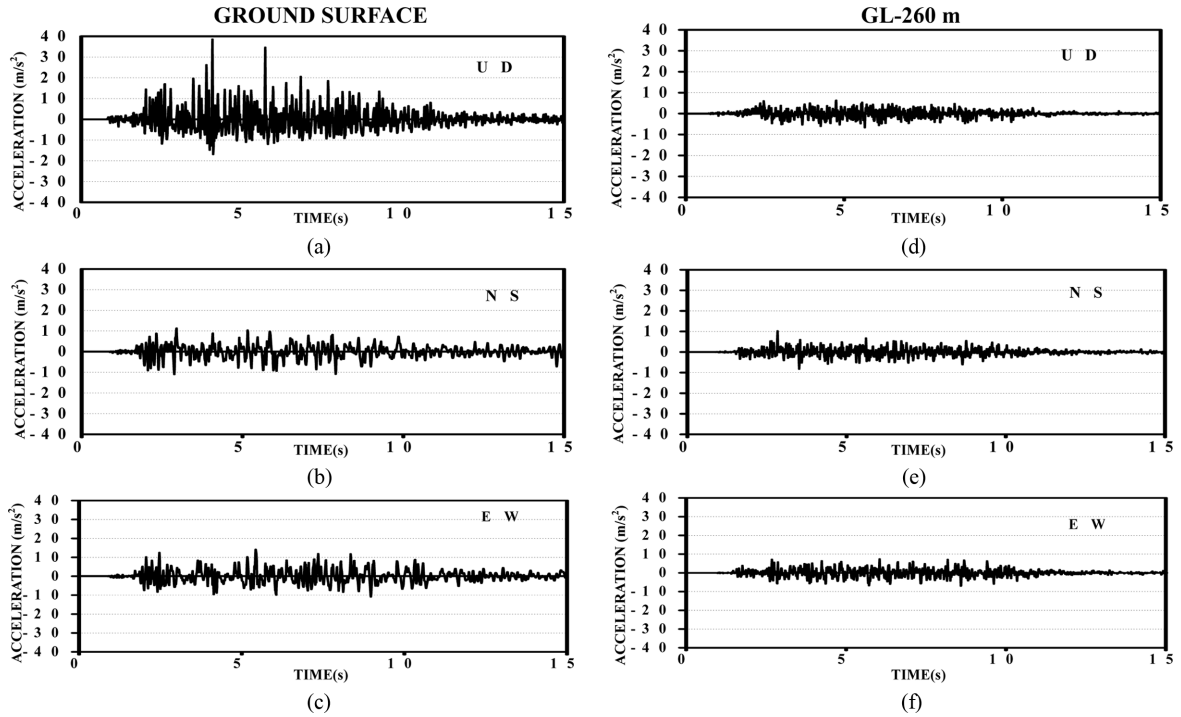

Fig. 2 Time histories of accelerations recorded at station IWTH25: (a) UD component, (b) NS component, (c) EW component at ground surface, (d) UD component, (e) NS component and (f) EW component at GL-260 m

Table 1 Peak acceleration records and occurrence time at ground surface and GL-260 m

Earthquake wave		Peak acceleration (m/s^2)	Occurrence time (s)
Ground surface	UD	38.66	4.08
	NS	11.43	2.95
	EW	14.33	5.43
GL-260 m	UD	6.81	5.65
	NS	10.36	2.83
	EW	7.48	6.05

The phenomenon of upthrow among ground layers or between a ground layer and structures is important. The aforementioned anomalous surface vertical acceleration records at station IWTH25 may be considered to be identical to the upthrown-boulder phenomenon for earthquake shaking. The origin of these phenomena is important because they have a significant influence on the earthquake resistance of soil and structures.

Aoi *et al.* (2008) reported a simple model of a mass bouncing on a trampoline to account for the asymmetric waveform and large amplification observed in the surface vertical acceleration records at station IWTH25 during the 2008 Iwate-Miyagi Nairiku earthquake. However, this model does not consider the ground conditions at station IWTH25. Moreover, the mechanism giving rise to such

trampoline behavior was not discussed.

Yamada *et al*. (2009) analyzed the difference between the ground surface and GL-260 m recordings for the vertical acceleration component at station IWTH25, and proposed a mechanism for the large vertical accelerations. They suggested that large upward acceleration is produced when a near-surface layer separates from a sublayer and then returns, striking the separated surface. Yamada *et al*. (2010) attempted to characterize nonlinear effects in near-surface soils during strong shaking by using deconvolved waveforms of KiK-net data. Yamada *et al*. (2010) estimated the shallow velocity structure around the station using microtremor measurements, and provided information on the spatial variation of the subsurface and the velocity structure, which is related to surface layer separation. The above studies clarified the singular surface vertical acceleration records at station IWTH25 from a seismological point of view. Although the occurrence of layer separation in the ground is likely due to vertical acceleration, the slapdown phase, in which a large upward spike in the surface vertical acceleration records is generated when the returning layer strikes the original separated surface, has not yet been clarified. The first question to be addressed is why the slapdown phases are not observed in the borehole vertical record of station IWTH25. Yamada *et al*. (2009) reported that the high-frequency waves may be strongly attenuated because the distance between the borehole accelerometer and the surface is significant. The second question to be addressed is why the large upward spikes observed in the vertical acceleration occur despite the very small degree of separation that occurs between the upper and lower layers.

Thus, physical evidence that may confirm the existence of layer separation and the singular surface vertical acceleration records at station IWTH25 has not yet been obtained. This is problematic from the points of view of structural engineering and earthquake resistance. Therefore, we propose a new mechanism for the jumping and collision of a ground layer and apply this mechanism to the vertical motion of a one-dimensional continuum subjected to the recorded vertical accelerations at GL-260 m.

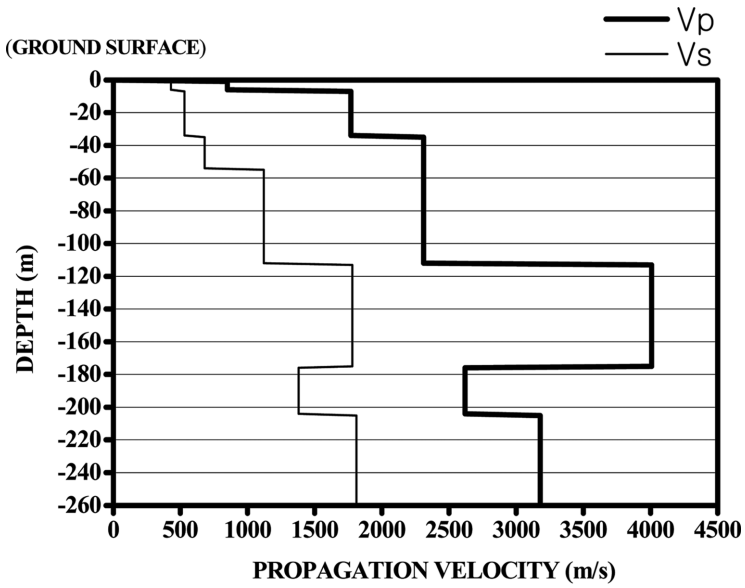

Fig. 3 Propagation velocities of the P and S waves from PS logging at station IWTH25

Table 2 Strata data at station IWTH25

Strata	Mass density [kg/m^3]	Thickness [m]	Depth [m]	V_p [m/s]	V_s [m/s]	Young's modulus E [GN/m^2]	Total stress σ_0 [kN/m^2]	Effective stress σ_V [kN/m^2]
Surface soil	1,800	1.0	1.0	850	430	0.883	17.6	7.8
Sedimentary soil	1,800	4.5	5.5	850	430	0.883	97.0	43.1
	1,800	28.5	34.0	1,770	530	1.46	599.8	266.6
Tuff	2,300	4.0	38.0	2,310	680	3.08	689.9	317.5
Tuff breccia	2,050	8.0	46.0	2,310	680	2.75	850.6	399.8
Sand	1,855	2.0	48.0	2,310	680	2.49	887.0	416.6
Sandy clay	1,800	2.0	50.0	2,310	680	2.41	922.3	432.3
Sand	1,855	4.0	54.0	2,310	680	2.49	995.0	465.8
Tuff breccia	2,050	10.0	64.0	2,310	1,120	6.92	1,195.9	568.7
Mudstone	2,100	48.0	112.0	2,310	1,120	7.09	2,183.7	1,086.1
Tuff breccia	2,050	63.0	175.0	4,010	1,780	17.8	3,449.4	1,734.4
Mudstone	2,100	1.0	176.0	2,620	1,380	10.4	3,470.0	1,745.2
Tuff breccia	2,050	28.0	204.0	2,620	1,380	10.2	4,032.5	2,033.3
Tuff	2,300	5.9	209.9	3,180	1,810	18.9	4,165.5	2,108.5
Tuff breccia	2,050	29.8	239.7	3,180	1,810	16.9	4,764.2	2,415.1
Mudstone	2,100	0.4	240.1	3,180	1,810	17.3	4,772.4	2,419.4
Tuff breccia	2,050	19.9	260.0	3,180	1,810	16.9	5,172.2	2,642.2

The aim of the present paper is to clarify the cause of the unprecedented large amplification and the asymmetric waveform for the surface vertical acceleration records at station IWTH25. We then show that there is a strong cause-and-effect relationship between unexpected landslides that occurred at numerous locations around the epicenter and the remarkably large vertical acceleration. The results suggest that, when designing earthquake-resistant structures, it is important to consider the effect of both vertical and horizontal motions.

2. Characteristics of the earthquake waveform recorded at station IWTH25

Station IWTH25, in West Ichinoseki, Japan, is part of the KiK-net system and is located 3 km from the epicenter of the 2008 Iwate-Miyagi Nairiku earthquake. The P- and S-wave propagation velocities obtained by PS logging are given in Fig. 3 and listed in Table 2.

Based on the boring log and PS logging, the Young's modulus of each ground layer is calculated as follows (Ohsaki 1991, 1994)

$$E = \rho V_s^2 \times \frac{3\left(\frac{V_p}{V_S}\right)^2 - 4}{\left(\frac{V_p}{V_S}\right)^2 - 1} \tag{1}$$

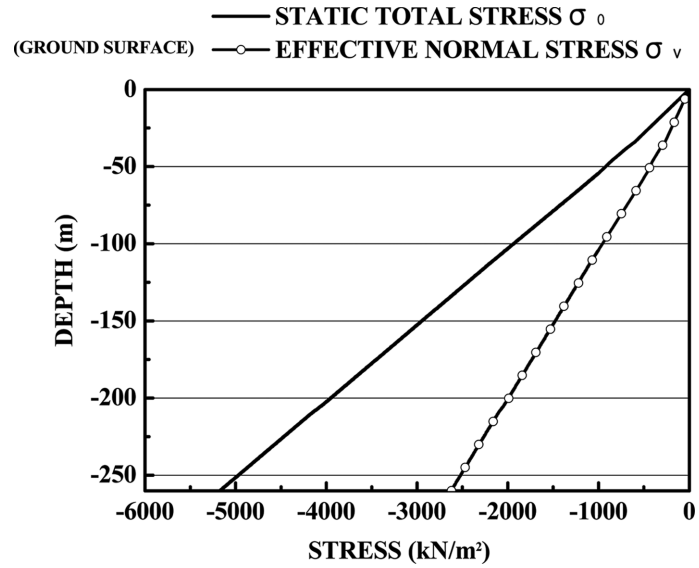

Fig. 4 Vertical distributions of effective stress and total static stress

Table 3 Natural frequencies

Mode	Vertical vibration (s)	Transverse vibration (s)
1st	0.416	0.678
2nd	0.190	0.317
3rd	0.114	0.188

where E represents the Young's modulus, and ρ is the mass density of each layer. Since the ρ value for the ground at West Ichinoseki is unclear, we use common values for the mass density.

The strata data at station IWTH25 are listed in Table 2. The ground water level at the time of the earthquake occurrence is unclear. However, since this station is located in the foothills, the ground water level is considered to be near the ground surface. Therefore, the stresses present are the total stress σ_0 and effective stress σ_v shown in Fig. 4 and listed in Table 2.

The natural frequencies for vertical and transverse free vibrations in the ground, which is regarded as a one-dimensional continuum, are listed in Table 3. These values are obtained from the NASTRAN FEM code. Figs. 5(a) through 5(c) show the Fourier spectra for the vertical, EW and NS components, respectively, of the ground surface acceleration records at station IWTH25. The predominant periods are 0.06, 0.11 and 0.09 s for the vertical, EW and NS components, respectively.

Figs. 6(a) through 6(d) indicate the acceleration response spectra and velocity response spectra of an elastic system using the vertical and EW horizontal surface accelerations records at GL-260 m, respectively, in which the damping constant h takes values of 0, 0.015 and 0.05. There are no noticeable differences between the vertical and horizontal acceleration response spectra. Figs. 7(a) through 7(d) show the acceleration response spectra and velocity response spectra obtained from

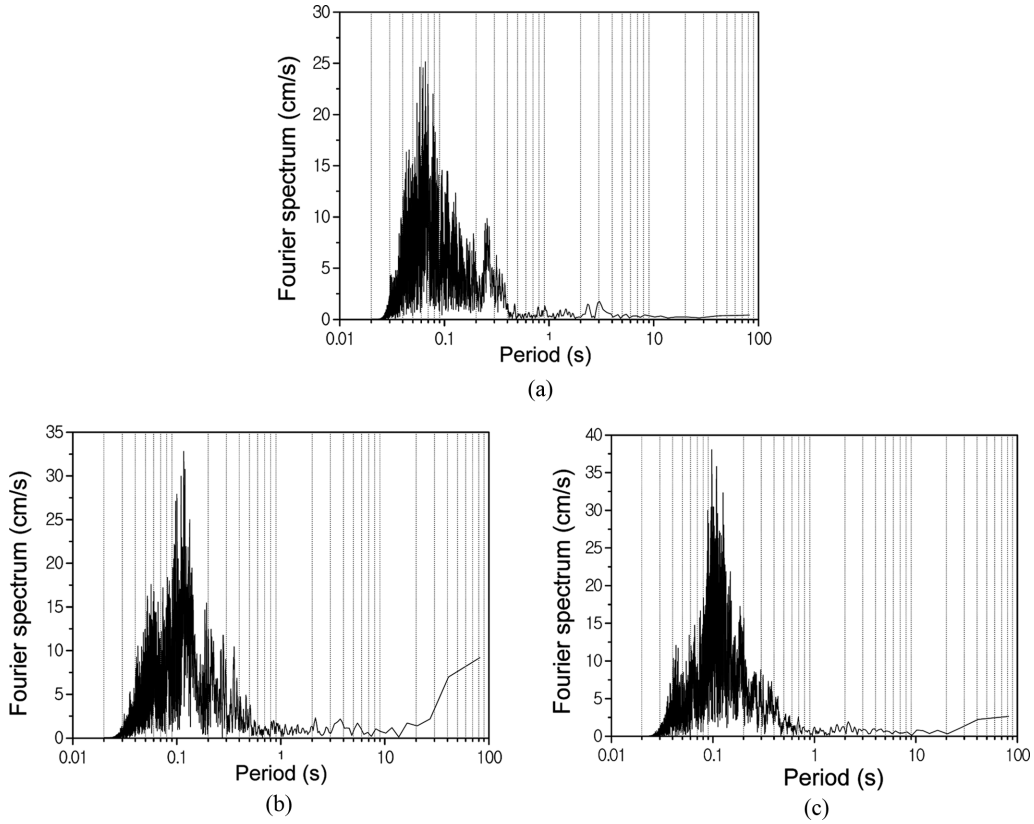

Fig. 5 Fourier spectra of (a) vertical, (b) EW and (c) NS components of the ground surface acceleration records at station IWTH25

the vertical and EW horizontal components, respectively, of the ground surface acceleration records at station IWTH25. The information obtained from these acceleration responses is restricted because these phenomena cannot be explained in terms of an elastic system, as described later herein.

3. Numerical model of vertical motion

Since the earthquake waves are recorded by two accelerometers located on the ground surface and at GL-260 m, the numerical calculation for the vertical motion uses a previously proposed one-dimensional continuum approach (Takabatake *et al.* 2008).

The depth of the ground is taken to be 260 m, and it is assumed to be composed of 16 bedding layers, based on the above-mentioned boring log. Since the propagation velocities of the P and S waves at GL-260 m are 3,180 and 1,810 m/s, respectively, we neglect the effect of ground below this level. Thus, the dynamic response is obtained by applying the acceleration recorded at GL-260 m to the base of the one-dimensional continuum. Since only the vertical motion is considered, the response results depend on the Young's modulus of the ground.

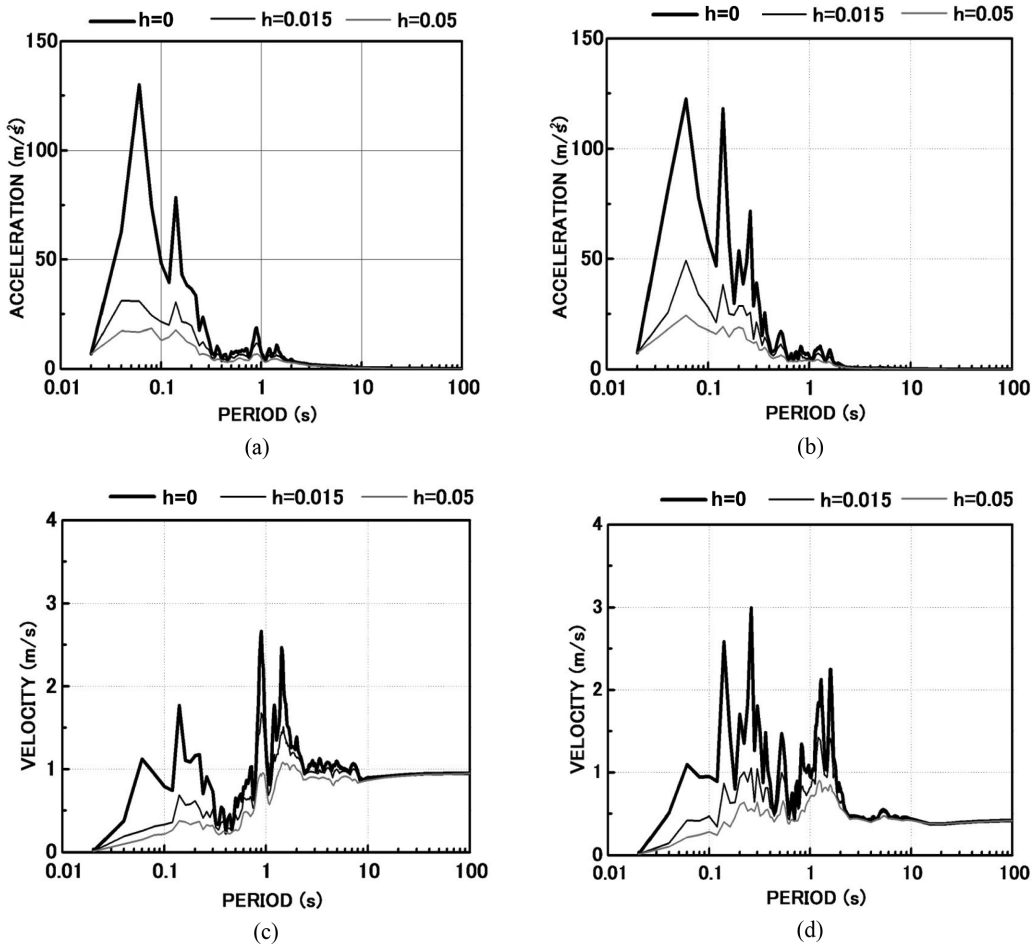

Fig. 6 Acceleration response spectra obtained from (a) vertical and (b) EW components recorded at GL-260 m and velocity response spectra obtained from (c) vertical and (d) EW components recorded at GL-260 m

4. Cause of the unprecedented 4 G vertical acceleration

The peak vertical acceleration recorded at the ground surface is approximately 4 G. The present study attempts to identify the cause of this acceleration based on the following hypotheses.

Hypothesis-1 The unprecedented vertical acceleration of 38.66 m/s^2 and the asymmetric waveform with large upward spikes at the ground surface were produced by the amplification effect of a vertical earthquake wave that propagated in the ground.

Since the boring log from GL-260 m to the ground surface is available, the ground is regarded as a one-dimensional continuum. Dynamic analysis of the vertical motion subjected to earthquake acceleration at GL-260 m, i.e., the ground base in the model, is carried out using explicit Dytran FEM code with a total of 2,616 beam elements. Each beam element is assumed to have a square

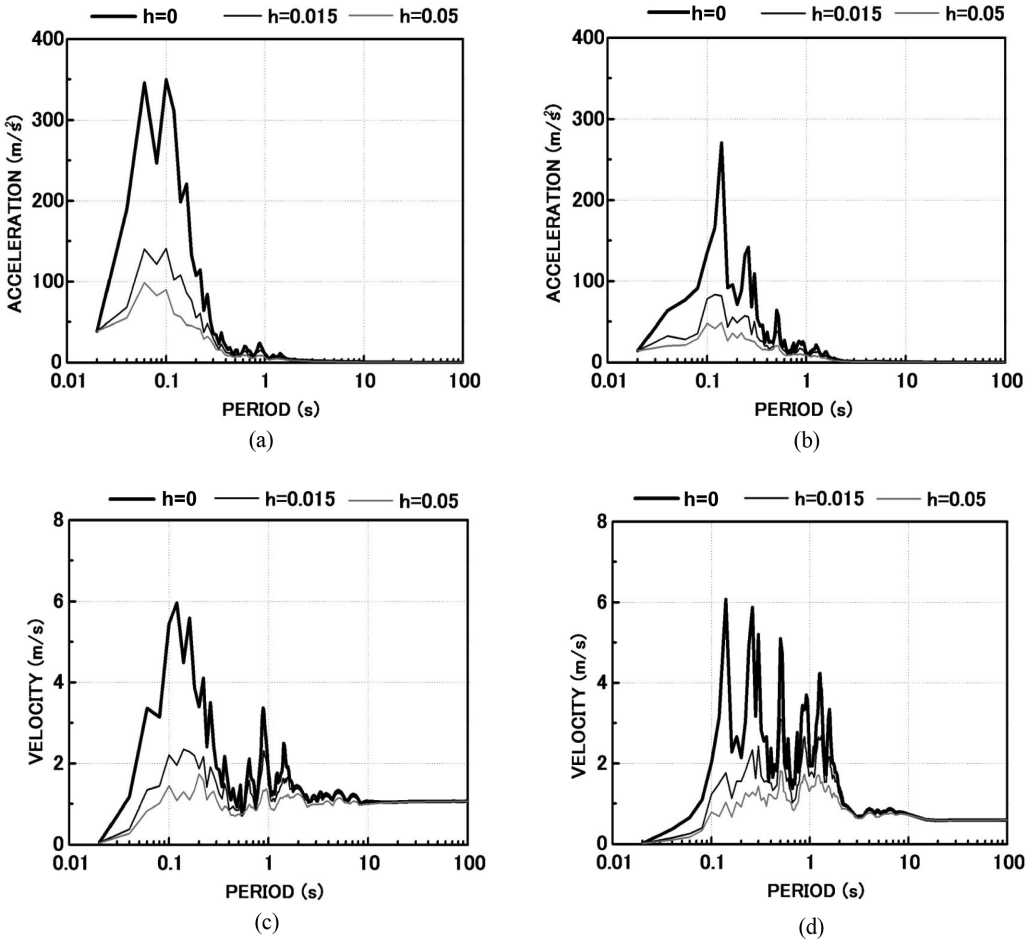

Fig. 7 Acceleration response spectra obtained from (a) vertical and (b) EW components recorded at ground surface and velocity response spectra obtained from (c) vertical and (d) EW components recorded at ground surface

cross section with sides of 10 m. Fig. 8 shows the time history of the vertical acceleration at the ground surface simulated using Dytran with $h = 0.015$ and recorded at station IWTH25. Based on the numerical results, the damping constant must be below 0.001 in order to cause the peak acceleration at the ground surface to exceed 4 G. However, the simulated waveform is always symmetric with respect to the zero axis and is distinctly different from the recorded waveform. Thus, *Hypothesis-1* cannot successfully account for the recorded waveform. Clearly, it is necessary to consider some particular behavior of the ground itself in order to explain the unprecedented acceleration recorded at the ground surface.

This idea is also supported by the response magnifications for the horizontal earthquake waves obtained using SHAKE. For the NS and EW horizontal components, the ground surface response magnifications are 0.76 and 0.72 times those at GL-260 m, respectively. The values obtained using SHAKE are always smaller than the recorded values and the surface horizontal accelerations are symmetric and resemble the recorded acceleration waves. Thus, the unprecedented surface vertical

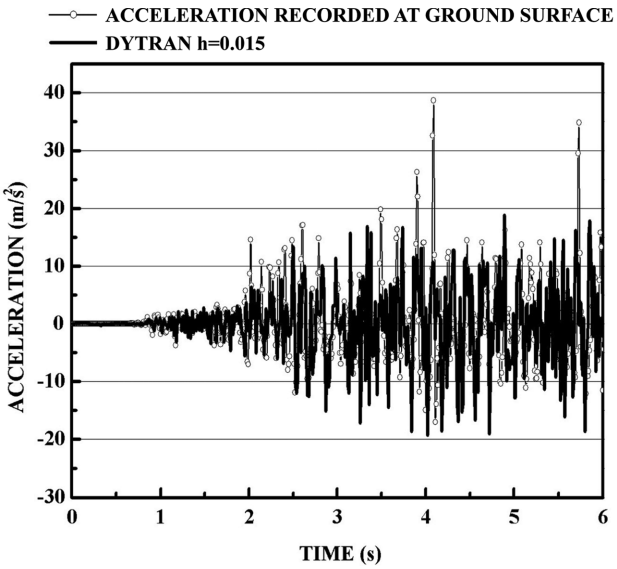

Fig. 8 Time histories of recorded surface vertical acceleration and surface vertical acceleration calculated using Dytran for h = 0.015

acceleration records also cannot be explained by general propagation of vertical earthquake waves. The failure of *Hypothesis-1* suggests that some effect originating in the ground must be examined.

We hereinafter discuss hypotheses based on a multi-degree-of-freedom (MDF) system for the ground. Therefore, we replace the one-dimensional continuum from GL-260 m to the ground surface with a MDF system consisting of 654 masses, as shown in Fig. 9(a). Figs. 10(a) and 10(b) show the vertical distributions of mass and stiffness, respectively. The distance between the masses is less than 0.4 m.

The equation of vertical motion for a MDF system, considering a static equilibrium state subjected to gravity, is as follows (Clough and Penzien 1975)

$$[M]\{\ddot{\bar{x}}\} + [C]\{\dot{\bar{x}}\} + [K]\{\bar{x}\} = -[M]\{\ddot{x}_0\} \tag{2}$$

where $[M]$, $[C]$ and $[K]$ are the mass matrix, the damping matrix and the stiffness matrix, respectively. The vertical coordinate axis x is measured from GL-260 m. The three matrixes are similar to those for the well-known MDF system subjected to lateral vibration because the form of the equation of vertical motion is the same as that of lateral motion. Here, $\ddot{\bar{x}}$, $\dot{\bar{x}}$ and $\bar{x}$ are the relative acceleration, relative velocity and relative displacement, respectively, which are measured from the static equilibrium state subjected to gravity. In addition, $\ddot{x}_0$ is the earthquake vertical acceleration at GL-260 m, recorded at station IWTH25.

Since the total number of masses in the MDF system is 654, the damping matrix $[C]$ is assumed to be approximately proportional to the initial stiffness as

$$[C] = \alpha[K] \tag{3}$$

where $\alpha = 2h_1/\omega_1$, (h_1 and ω_1 are the damping constant and vertical natural frequency,

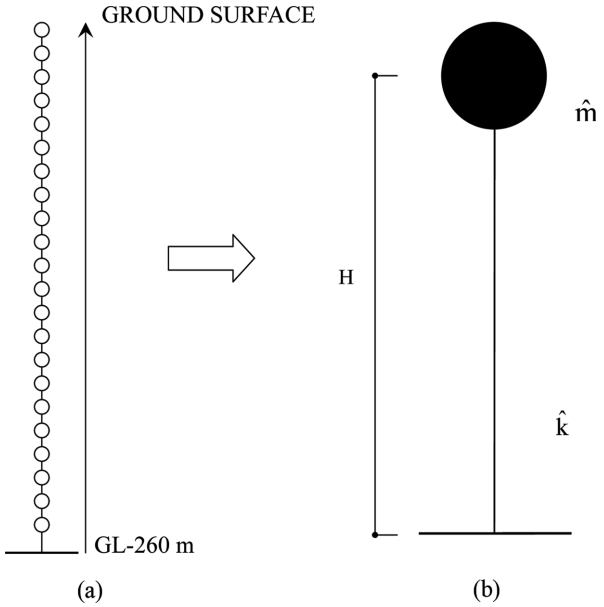

Fig. 9 Lumped-stiffness modeling: (a) multi-degree-of-freedom (MDF) system and (b) equivalent single-degree-of-freedom system (ESDF)

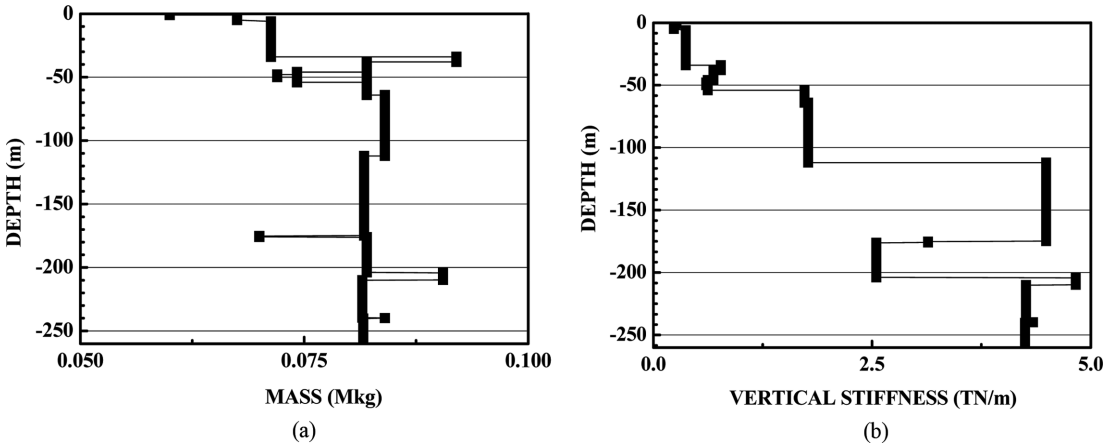

Fig. 10 Vertical distributions of (a) mass in MDF system and (b) vertical stiffness in MDF system

respectively, for the first mode). We found that there is no difference between the numerical results obtained using Eq. (3) and the Rayleigh damping equation, given by

$$[C] = \alpha[M] + \beta[K] \tag{4}$$

Hypothesis-2 The unprecedented vertical acceleration at the ground surface is caused by nonlinear behavior of the ground stiffness.

This hypothesis is based on nonlinear behavior of the stress-strain relationship for the ground

when subjected to earthquake vertical action.

To perform a simple evaluation of the effects of ground vertical stiffness variations over time, we replaced the current MDF system with an equivalent single-degree-of-freedom (ESDF) system, as shown in Fig. 9(b). The equivalent mass $\hat{m}$ is 2.969×10^7 kg, and the equivalent elastic stiffness $\hat{k}$ is 1.958×10^9 N/m.

The equation of vertical motion for the ESDF system is given as follows

$$\hat{m}\ddot{\bar{x}} + \hat{c}\dot{\bar{x}} + k(x)\bar{x} = -\hat{m}\ddot{x}_0 \tag{5}$$

where $\bar{x}$, $\dot{\bar{x}}$ and $\ddot{\bar{x}}$ are the relative vertical displacement, relative velocity and relative acceleration, respectively, $\ddot{x}_0$ is the vertical acceleration recorded at GL-260 m, and $k(x)$ is the nonlinear stiffness of the equivalent system. The absolute vertical displacement x, which is measured from the static equilibrium state (without earthquake action), is the sum of the vertical displacement x_0 at GL-260 m and the relative displacement $\bar{x}$

$$x(t) = x_0(t) + \bar{x}(t) \tag{6}$$

From Eq. (5), the nonlinear stiffness k is obtained from

$$k = \frac{-\hat{m}\ddot{x}_0 - \hat{m}\ddot{\bar{x}} - \hat{c}\dot{\bar{x}}}{\bar{x}} \tag{7}$$

In the above equation, the borehole acceleration records $\ddot{x}_0$ at GL-260 m and the acceleration records $\ddot{\bar{x}}$ at the ground surface at station IWTH25 are known. In addition, the relative vertical velocity $\dot{\bar{x}}$ and the relative vertical displacement $\bar{x}$ are determined by integrating the accelerations $\ddot{\bar{x}}$. Hence, the time history of the stiffness k may be obtained from Eq. (7). In order to clarify the nonlinear characteristics of k explicitly, we define the stiffness ratio η ($\eta = k(x)/\hat{k}$), where $\hat{k}$ is the known elastic stiffness of the ESDF system. When $\eta = 1$, the ESDF system can be considered to be

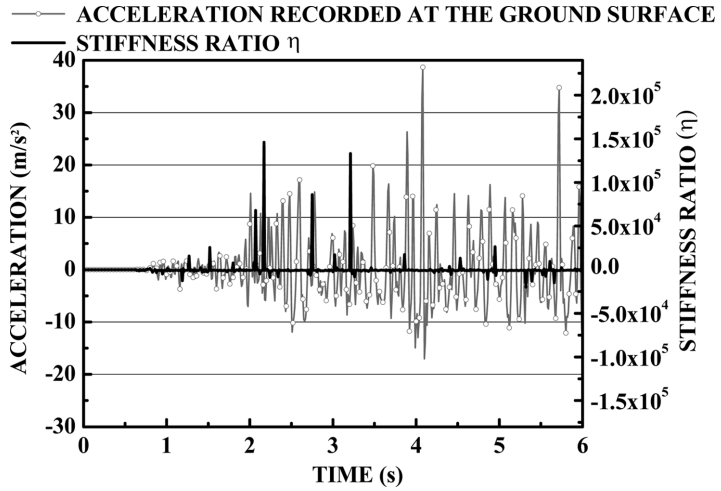

Fig. 11 Time histories of surface vertical acceleration and stiffness ratio

elastic. $\eta > 1$ means that stiffness of the ground indicates stronger. Conversely, $\eta < 1$ means that stiffness of the ground indicates weaker. The case of $\eta > 1$ is not valid for normal compacted ground. Fig. 11 shows the time histories of the surface vertical acceleration recorded at station IWTH25 and the stiffness ratio η. The left vertical axis indicates the absolute acceleration and the right vertical axis denotes the stiffness ratio η.

From Fig. 11, before 4.08 s, at which the peak vertical acceleration of 38.66 m/s^2 occurs at the ground surface, the stiffness ratio is seen to be approximately 150,000. However, for normal compacted ground, the stiffness ratio cannot physically take values greater than unity, because the nonlinear behavior of soil results in low stiffness. Hence, such extremely large vertical stiffness values cannot be obviously produced by the physical nonlinearity of the ground. If the nonlinear relationship of the ground has an important part in the problem considered herein, then the stiffness ratio must be less than one. Thus, *Hypothesis-2* does not hold.

Hypothesis-3 The unprecedented vertical acceleration at the ground surface is caused by an additional external force, which is produced by a propagation process due to earthquake vertical motion.

The failure of *Hypothesis-2* suggests the occurrence of some additional force in the ground. Therefore, we rewrite Eq. (5) for the aforementioned ESDF system as Eq. (8), in which the equivalent stiffness $\hat{k}$ is assumed to be elastic and the additional force p_{add} is defined as being upwardly positive along the vertical coordinate axis x and depends on time.

$$\hat{m}\ddot{\bar{x}} + \hat{c}\dot{\bar{x}} + \hat{k}\bar{x} = -\hat{m}\ddot{x}_0 + p_{add}(t) \tag{8}$$

From Eq. (8), $p_{add}(t)$ is obtained as

$$p_{add}(t) = \hat{m}\ddot{\bar{x}} + \hat{c}\dot{\bar{x}} + \hat{k}\bar{x} + \hat{m}\ddot{x}_0 \tag{9}$$

Since the right-hand side of the above equation is known, the time history of $p_{add}(t)$ may be obtained. Then, in order to clarify the physical properties of the additional force, the additional acceleration $\ddot{x}_{add}(t)$, obtained by dividing $p_{add}(t)$ by the equivalent mass $\hat{m}$, is

$$\ddot{x}_{add}(t) = \frac{P_{add}(t)}{\hat{m}} \tag{10}$$

Fig. 12 shows the time history of $\ddot{x}_{add}(t)$ and the acceleration recorded at the ground surface; the curves are seen to be in fairly good agreement.

The above numerical results indicate that an additional force P_{add} acting in the upward direction in the ESDF system is necessary in order to produce a surface vertical acceleration of approximately 4 G. It is reasonable that this force is produced by earthquake wave propagation in the ground. This additional force is equal to the magnitude of the equivalent mass multiplied by the surface vertical acceleration. The additional absolute acceleration $\ddot{x}_{add}(t)$ is given by

$$\ddot{x}_{add}(t) = \ddot{x}_0(t) + \ddot{\bar{x}}(t) \tag{11}$$

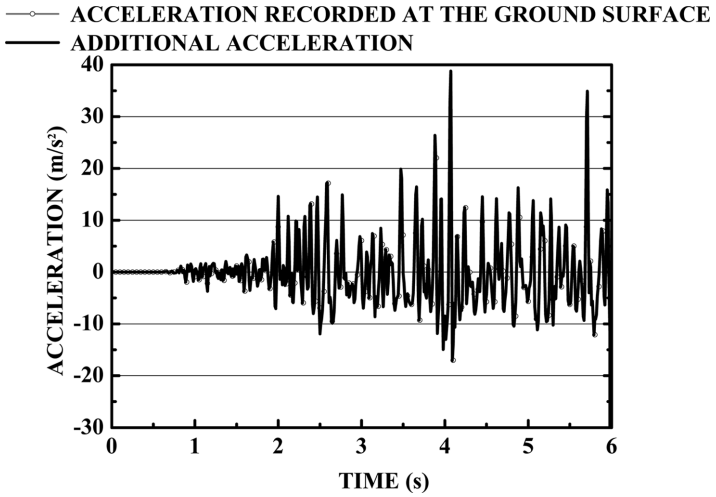

Fig. 12 Time histories of additional acceleration and surface vertical acceleration

Thus, the problem is reduced to how to determine the mechanism responsible for this additional force.

Hypothesis-4 The additional force required to cause the surface vertical acceleration at station IWTH25 is produced by collision with an adjacent mass due to local jumping of some ground layer as a result of the earthquake action. This collision is produced by an upward movement, with no gaps occurring between the adjacent non-jumping mass and the jumping mass.

In order to examine the appropriateness of this hypothesis, we define the jumping mass conditions in the aforementioned MDF system consisting of 654 masses. For any given mass to jump, the following three conditions must be simultaneously satisfied: (1) the mass is in a tensile state due to vertical stress, which overwhelms the static total stress σ_0, or the static effective stress σ_v; (2) the mass is accelerated upward in absolute coordinates at 1 G (9.8 m/s^2) or greater, which compensates for the effect of gravity and (3) the velocity of the mass is directed upward.

When a mass satisfies these conditions, it jumps instantaneously and collides with the adjacent non-jumping mass, which is located above it. Fig. 13 shows the additional force $\overline{P}_i$ produced by a collision due to such jumping. When the (i-1)-th mass jumps, the i-th non-jumping mass, which lies directly above it, is subjected to the following additional force $\overline{P}_i$

$$\overline{P}_i = \frac{m_i}{m_i + m_{i-1}}(\ddot{x}_{i-1} - \ddot{x}_i)(1+e)\cdot m_i > 0 \tag{12}$$

where $\ddot{x}_i$ and $\ddot{x}_{i-1}$ are the absolute accelerations of the i-th and (i-1)-th masses, respectively, e is the coefficient of restitution between the i-th mass and the (i-1)-th mass. Eq. (12) is derived from the well-known stereomechanical collision, as shown in Goldsmith (2001). Only non-jumping mass or masses that are located directly above jumping masses are affected by such collisions. Due to this collision, an additional force is applied in turn to all of the non-jumping masses in the group overlying directly the original jumping mass, causing this group to simultaneously jump. It means

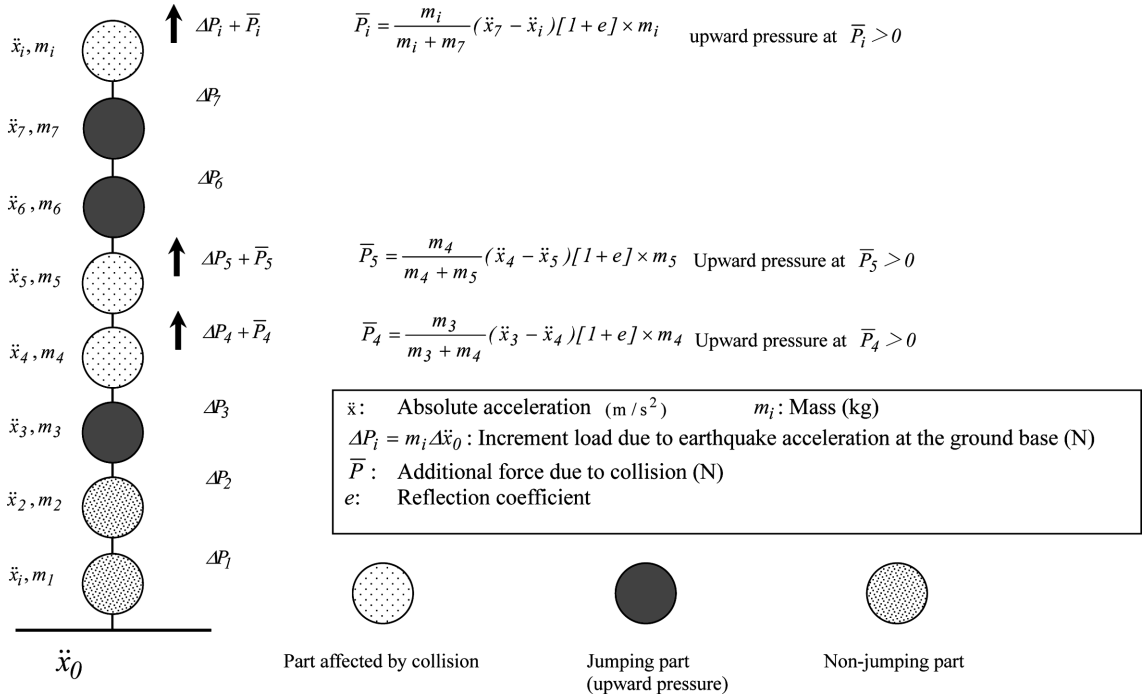

Fig. 13 Additional impact force $\overline{P}_i$ due to jumping mass or masses

this additional force is not applied to the non-jumping masses in the group overlying undirectly the original jumping mass. This action is assumed to propagate in a chain-like manner and, for simplicity, any time lag is neglected. It is also assumed that the jumping mass instantly recontacts the lower mass after jumping and the additional instantaneous acceleration, the instantaneous velocity increment, and the instantaneous displacement increment are zero while jumping.

Based on the above assumptions, a dynamic vertical response analysis was carried out for the MDF system. The dynamic analysis used constant acceleration methods with a time step of 0.0001 s. Numerical computations revealed that the jumping location and occurrence time depend on the magnitude of the damping constant, h. In the case of actual ground, the damping constant differs according to the ground layer. However, for simplicity, we assume the same value for all layers. In addition, the coefficient of restitution e is assumed to be unity, corresponding to perfect elasticity. The simulations were carried out for damping constant values in the range 0.01 to 0.02. Figs. 14(a) and 14(b) show the simulated temporal variation of the absolute acceleration at the ground surface for h = 0.015, where the effective stress and total static stress, respectively, are used as the ground static stress. In these figures, the accelerations suddenly increase after approximately 6 s. The acceleration differs significantly from that actually recorded at the ground surface. The primary reason for this difference is considered to be the assumption that the damping constant is invariant in the numerical calculations. When a mass jumps, the continuity of the ground instantaneously drops at that position, and wave propagation in the ground suddenly decreases. Consequently, the damping constant for the entire ground increases and the vibration decreases. Therefore, the volume of ground in which jumping occurs decreases. For the above reasons, the difference in the magnitude of surface accelerations between the numerical results and the records has no important

meaning. Further numerical simulations for times earlier than 6 s. may clarify the effects of jumping.

Figs. 14(c) and 14(d) show the time histories of layer jumping corresponding to Figs. 14(a) and 14(b), respectively, for h = 0.015. Figs. 14(a) and 14(c) show the numerical results obtained using the effective stress σ_V for the static stress in the ground. On the other hand, Figs. 14(b) and 14(d) show numerical results obtained using the total static stress σ_0 for the static stress. Figs. 14(c) and 14(d) show that for h = 0.015, jumping occurs at shallow layers located within a depth of 10 m from the ground surface. The difference between Figs. 14(c) and 14(d) depends on the water level depth. The depth of the jumping layer obtained from the effective stress increases discontinuously with time, as shown in Fig. 14(c). On the other hand, the depth of jumping layer determined using the static stress exhibits the opposite behavior, as shown in Fig. 14(d). The practical depth of the jumping layer is considered to be halfway between the ground surface and a depth of 10 m, because the water level depth is unknown. Moreover, the acceleration recorded at the ground surface decreases after 4.08 s.

Furthermore, numerical calculations in which the damping constant was varied revealed that the

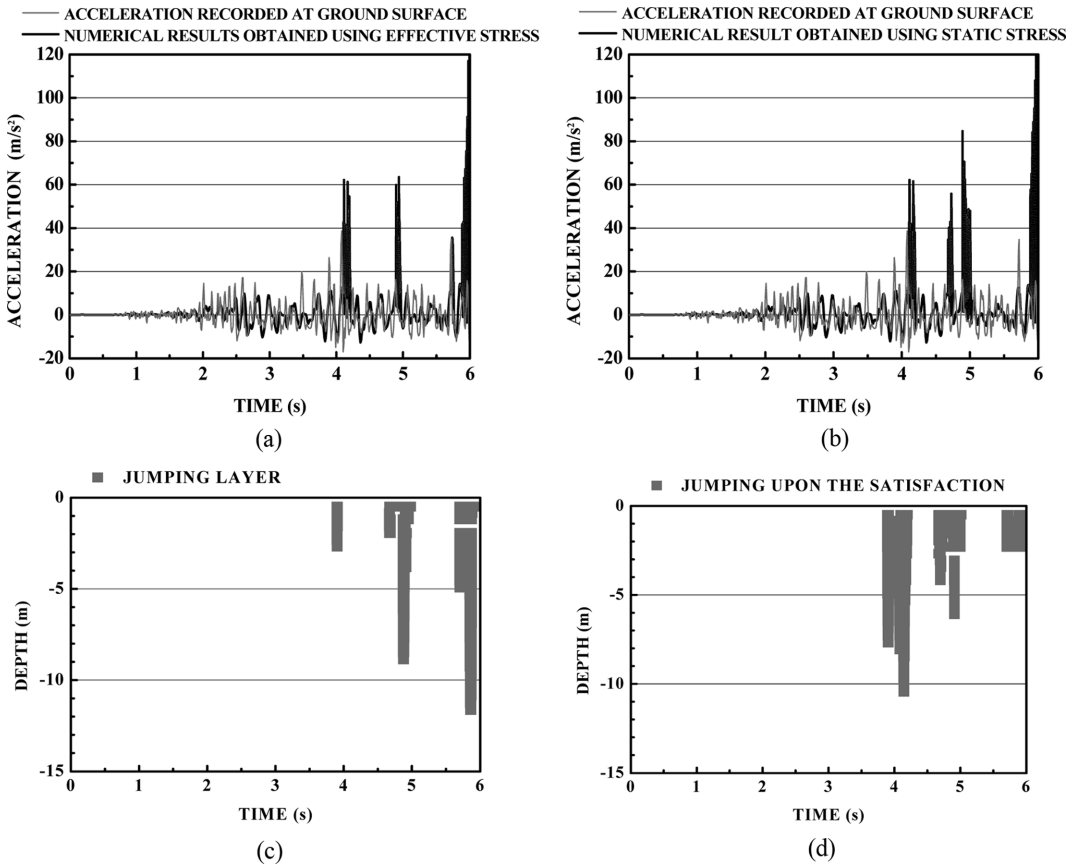

Fig. 14 Time histories of surface vertical acceleration and numerical results based on (a) effective stress, (b) total static stress and jumping layer based on, (c) effective stress and (d) total static stress for h = 0.015

depth of the jumping layer increases as the damping constant increases. The times at which jumping occurred were found to be closely correlated to the occurrence of the large upward spikes in the surface vertical acceleration records, regardless of the damping constant (in the range 0.01 to 0.02).

As shown in Fig. 14(a), the acceleration response at approximately 4 s based on the effective stress is 61.0 m/s^2, which is 1.6 times greater than the vertical acceleration of 38.6 m/s^2 recorded at station IWTH25. On the other hand, that based on the total static stress is 62.0 m/s^2, as shown in Fig. 14(b).

The time history of the acceleration shown in Fig. 14(a) agrees well with the waveform of the surface vertical acceleration records before 5 s, except for the peak values. In particular, the waveform obtained here is closely correlated with the large upward spikes in the surface vertical acceleration records.

Since the present paper assumes that the ground is continuous and contains no gaps, the collisions are considered to involve simple pushing of the upper layers by the layer that undergoes jumping. However, in practice, some gaps may exist between colliding layers. In such a case, the practical action produced by a collision is expected to be smaller than when no such gap exists. The additional force given by Eq. (9) is considered to become smaller in such a situation; however, this mechanism is not taken into consideration in the present paper.

As mentioned above, although the mechanism proposed herein requires further consideration of the additional force produced by the collision, the cause of the unprecedented vertical acceleration during the 2008 Iwate-Miyagi Nairiku earthquake can be rationally explained by the jumping and collision of ground layers.

In the above response analysis, the stiffness k in the vertical direction is calculated based on an elastic foundation. This assumption is valid because the order of the maximum strain in the first 6 s. is less than 10^{-4}, as shown in Fig. 15. Note that the analytical method proposed here is basically nonlinear because jumping and collision of adjoining ground layers are considered based on an elastic foundation.

Moreover, the waveform recorded at the surface could never be produced unless such jumping and collisions are considered, and the stiffness in the vertical direction is considered from the

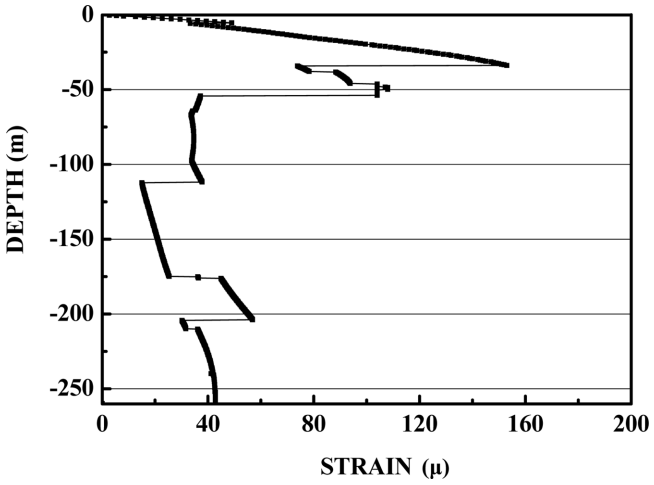

Fig. 15 Distribution of maximum strain in first 6 s

viewpoint of elasto-plasticity. This is also clear from the continuum analysis performed using Dytran.

The validity of *Hypothesis-4* was also confirmed experimentally, as described below. In an earthquake that occurred in Mexico in 1940, collisions between adjoining buildings were found to have caused serious damage (Jankowski 2005). Therefore, as shown in Fig. 16, we experimentally investigated collisions due to the dynamic response of two frame structures connected by an expansion joint to horizontal motion caused by an earthquake. Two four-story frame structures having the same stiffnesses but different masses were placed on a shaker table. Figs. 17(a) and 17(b) show the variation with time of the absolute acceleration recorded at the top floors of the two frames, when subjected to excitation corresponding to the El-Centro 1940 NS wave, normalized to a maximum velocity of 0.5 m/s. Whenever two buildings repeatedly collide at the expansion joint, the acceleration waveform is asymmetric and exhibits large spikes. This behavior is strikingly similar to

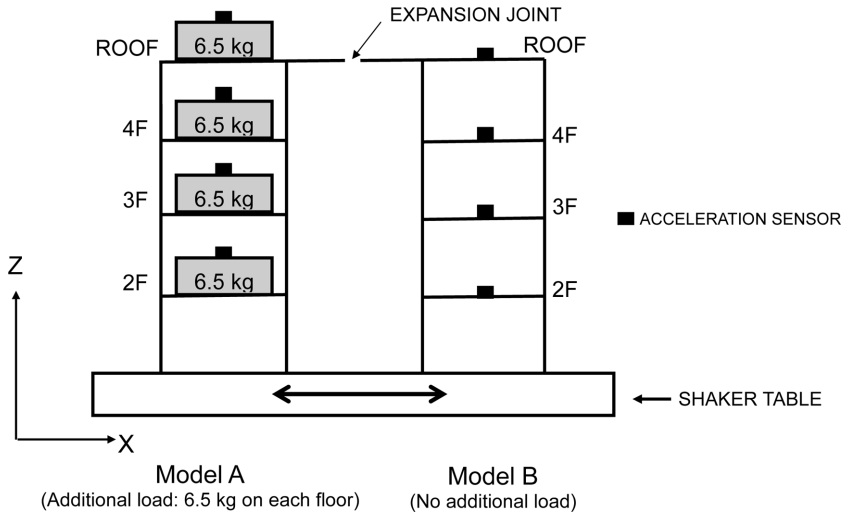

Fig. 16 Pounding tests for Model A and Model B

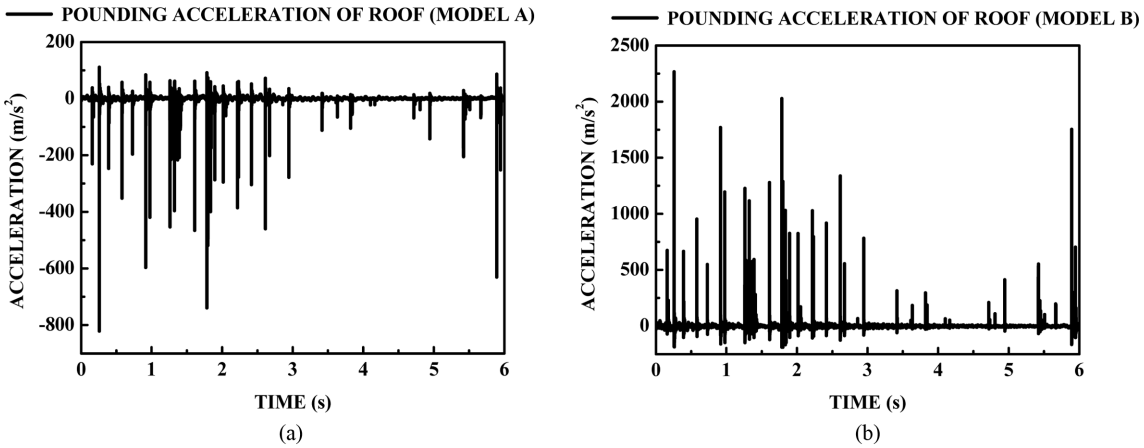

Fig. 17 Time history of acceleration at each roof floor of (a) Model A and (b) Model B

the characteristics of the surface vertical acceleration records at station IWTH25 for the 2008 Iwate-Miyagi Nairiku earthquake, thus supporting the validity of *Hypothesis-4*.

The present study was based on the simple assumption of the jumping and collision of ground layers based on lumped mass. More specifically, an analytical method involving wave propagation is considered by regarding the ground as a one-dimensional continuum. Recently, Cole *et al*. (2010) discussed the effects of the mass distribution on the pounding together of two adjacent buildings.

5. Seismic countermeasures to vertical ground motion

One characteristic of the damage inflicted by the 2008 Iwate-Miyagi Nairiku earthquake was the occurrence of large-scale landslides in many places. When structures are subjected to large vertical ground motion, an upward force is applied to them. This gives rise to a reduction in the amount of friction between the ground and foundations of the structure. In general, the horizontal resistance force Q_F at the foundation is expressed by multiplying the vertical force N due to the weight of the structure by the horizontal friction coefficient μ between the foundation and ground, as follows

$$Q_F = N \cdot \mu \tag{13}$$

If the horizontal friction coefficient μ is constant, then a reduction in the vertical force N due to vertical ground motion reduces the resistance Q_F. Since the force along a slope always acts in the direction of the slope, the decrease in the horizontal resistance force Q_F due to the vertical ground motion increases the risk of slope collapse for a layer with a low friction coefficient. Once collapse occurs at some layer, large-scale collapse then follows. The jumping of a layer near the ground surface reduces the resistance along the slope, which is considered to induce large-scale collapse of the slope.

Although the main influence of an earthquake on a structure is the horizontal ground motion, the occurrence of jumping phenomena between the structure and the ground is considerable for vertical accelerations of about 1 G. In particular, for a slope composed of a shallow layer with a low friction coefficient, the use of an earth-anchor would be effective for preventing jumping of the weak layer due to vertical ground motion.

Due to the difference in the wave velocities of horizontal and vertical ground motions, the peak times do not agree at locations far from the source. However, near the source, the difference in the peak times is very small. In addition, when the magnitude of the earthquake is very large, vertical ground motion is considered to have a significant influence on the structure during periods of peak horizontal ground motion. Therefore, in structural design, it is necessary to consider the reduction of horizontal resistance that occurs due to such vertical ground motion.

6. Conclusions

We carried out various numerical simulations to clarify the cause of the unusual asymmetric vertical acceleration waveform with large upward spikes, recorded at the ground surface by the accelerometers at station IWTH25 during the 2008 Iwate-Miyagi Nairiku earthquake.

The irregularity of the waveform can be explained by a mechanism of jumping and collision of

soil masses within the ground. Although the mechanism proposed herein cannot completely explain the behavior of the waveform, we have presented a physical explanation for the singular surface vertical acceleration records obtained at station IWTH25.

References

Aoi, S., Kunugi, T. and Fujiwara, H. (2008), "Trampoline effect in extreme ground motion", *Science*, **322**(5902), 727-730.

Cole, G., Dhakal, R., Carr, A. and Bull, D. (2010), "An investigation of the effects of mass distribution on pounding structures", *Earthq. Eng. Struct. D*., **40**(5), 641-659.

Clogh, R.W. and Penzien, J. (1975), *Dynamic of structures*, McGraw-Hill.

Editorial Community of Handbook of soils and foundations (1999), *Handbook of soils and foundations (in Japanese)*, The Japanese Geotechnical Society.

Goldsmith, W. (2001), *Impact*: *The theory and physical behaviour of colliding solids*, Dover Publications, Inc., New York.

Jankowski, R. (2005), "Non-linear viscoelastic modeling of earthquake-induced structural pounding", *Earthq. Eng. Struct. D*., **34**(6), 595-611.

K-net and KiK-net station. (2008), http://www.kik.bosai.go.jp/kik, National Research Institute for Earth Science and Disaster Prevention.

Ohsaki, Y. (1991), *Foundation of structures (in Japanese)*, Gihodo.

Ohsaki, Y. (1994), *New introduction of spectrum analysis for earthquake (in Japanese)*, Kashima Press.

Paz, M. (1991), *Structural dynamics*, 3rd ed., Van Nostrand Reinhold, New York.

Tahghighi, H. (2011), "Earthquake fault-induced surface rupture-A hybrid strong ground motion simulation technique and discussion for structural design", *Earthq. Eng. Struct. D*., **40**(5), 1951-1608.

Tothong, P. and Cornell, C.A. (2008), "Structural performance assessment under near-source pulse-like ground motions using advanced ground motion intensity measures", *Earthq. Eng. Struct. D*., **37**(7), 1013-1037.

Yang, D., Pan, J. and Li, G. (2009), "Non-structure-specific intensity measure parameters and characteristic period of near-fault ground motions", *Earthq. Eng. Struct. D*., **38**(11) 1257-1280.

Yamada, M., Mori, J. and Heaton, T. (2009), "The slapdown phase in high-acceleration records of large Earthquake", *Seismol. Res. Lett*., **80**(4), 559-564.

Yamada, M., Yamada, M., Hada, K., Ohmi, S. and Nagao, T. (2010), "Spatially dense velocity structure exploration in the source region of the Iwate-Miyagi Nairiku earthquake", *Seismol. Res. Lett*., **81**(4), 597-604.

Yamada, M., Mori, J. and Ohmi, S. (2010), "Temporal changes of subsurface velocities during strong shaking as seen from seismic interferometry", *J. Geophys. Res*., **115**(B03302), 1-10.

Takabatake, H., Mukai, H. and Hirano, T. (1993), "Doubly symmetric tube structures II: Dynamic analysis", *J. Struct. Eng.-ASCE*, **119**(7), 2002-2016.

Takabatake, H., Nonaka, T. and Umeda, Y. (2008), "Implications of thrown-out boulders for earthquake shaking", *J. Earthq. Eng*., **12**(8), 1325-1343.

IT